

Assembly of Two-Dimensional DNA Arrays Could Influence the Formation of Their Component Tiles

Victoria E. Paluzzi,^[a] Cuizheng Zhang,^[a] and Chengde Mao^{*[a]}

Tile-based DNA self-assembly is a powerful approach for nanoconstructions. In this approach, individual DNA single strands first assemble into well-defined structural tiles, which, then, further associate with each other into final nanostructures. It is a general assumption that the lower-level structures (tiles) determine the higher-level, final structures. In this study, we

present concrete experimental data to show that higher-level structures could, at least in the current example, also impact on the formation of lower-level structures. This study prompts questions such as: how general is this phenomenon in programmed DNA self-assembly and can we turn it into a useful tool for fine tuning DNA self-assembly?

Introduction

DNA self-assembly provides a powerful approach for nanoconstructions.^[1–7] One strategy of the DNA self-assembly centers on DNA tiles.^[8–12] Individual DNA single strands first assemble into well-defined structural tiles, which, then, further associate with each other into final nanostructures. This strategy has allowed assembly of a wide range of DNA nanostructures from discrete objects to extended arrays.^[13–23] In the tile-based DNA assembly, the final structures can be precisely predicted from the tile structures and the tile structures have no change during the final structure formation.^[8] Here, we report a case study that the final DNA structures impact on the tile formation. Similar phenomena have been observed before in other molecular systems. For example, it is not uncommon that crystals packing changes the structure of the molecules to be crystallized.^[24,25] However, our observation, to the best of our knowledge, is the first report for programmed DNA self-assembly and may also suggest that it could provide a novel design strategy for programmed DNA self-assembly.

This study utilizes a DNA homo-oligomerization system based on the branched Kissing Loop (bKL) motif. Homo-oligomerization is a common strategy to form large protein complexes in nature due to its simplicity.^[26] It reduces synthesis errors,^[27] minimizes coding space,^[28] and effectively regulates large assemblies.^[26] It also inspires a minimalist's approach for assembly of complicated DNA nanostructures.^[29] For one single DNA component to assemble into non-linear structures, it needs at least three interacting sites. Its two ends could potentially be involved in sticky-end cohesion, then one more

interacting site must be internal and should not involve a free end. Such internal elements are very limited for DNA with two noticeable examples of the paranemic crossover (PX) motif and the bubble-bubble interaction,^[30,31] which are relatively large motifs. Recently, a small bKL interaction has been designed for RNA self-assembly by modeling common RNA KL interactions.^[32] Such bKL interactions provide a convenient way for DNA homo-polymerization.

Results and Discussion

A bKL interaction involves two DNA duplex molecules: one with a 6-nucleotide (nt) bulge and the other one with a 9-nt hairpin loop (Figure 1c, 6-nt base-pairing region, red; A3-region, green). If the two single-stranded regions have complementary sequences [the hairpin loop has three extra adenines (A) at the 5', Figure S1], they will base pair with each other to form a half-turn duplex and bring the two DNA duplex molecules together, resulting in a 3-way junction (Figure 1a). It is a branched structure, thus being named as branched Kissing Loop interaction, in contrast to the coaxial stacking architecture of the conventional RNA kissing loop interaction. The overall architecture of a bKL motif closely resembles the structure of a T-junction motif (Figure 1b), a previously reported DNA motif.^[34] Though both motifs provide cohesion between two molecules, a major difference exists between the two motifs in terms of the involvement of free DNA ends at the interaction interfaces. A bKL requires no free end, but a T-junction critically depends on two free ends. Thus, bKLs allow two DNA molecules to interact with each other by internal elements while T-junctions cannot. Internal interactions (involving no free end) are the key for folding long strand into defined structures without helping strands.^[31,35] In this study, the T-junction was used as a reference because of its close, architectural similarity to bKL.

Motifs K1 and T1 were designed for homo-oligomerization via bKL and T-junction cohesion, respectively (Figure 1). Both motifs have a semi-rigid L-shape. Each motif contains one complementary interaction pair located at its top and lower left corner. In addition, there is an inert end at the lower right for

[a] V. E. Paluzzi, C. Zhang, C. Mao
Department of Chemistry
Purdue University, West Lafayette, IN-47907 (USA)
E-mail: mao@purdue.edu

Supporting information for this article is available on the WWW under <https://doi.org/10.1002/cbic.202200306>

© 2022 The Authors. ChemBioChem published by Wiley-VCH GmbH. This is an open access article under the terms of the Creative Commons Attribution Non-Commercial License, which permits use, distribution and reproduction in any medium, provided the original work is properly cited and is not used for commercial purposes.

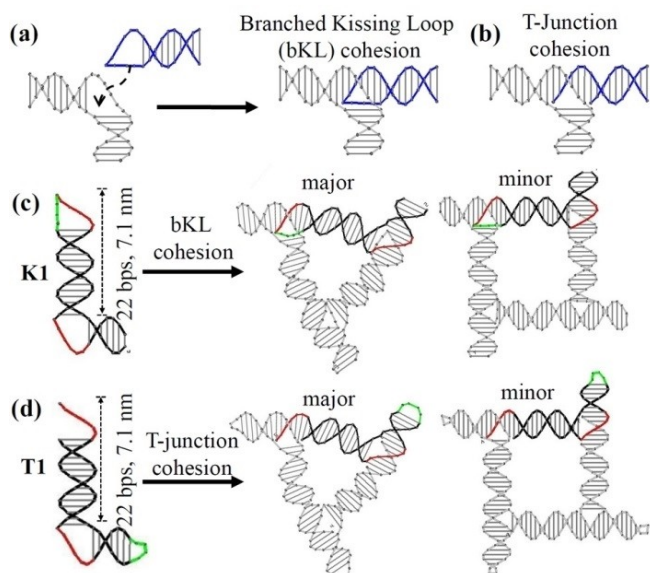


Figure 1. Branched Kissing Loop (bKL) for DNA self-assembly. Schemes of (a) bKL cohesion (with no free-end) vs. (b) T-junction cohesion (with a free-end). Both involving the formation of a half-turn DNA duplex. Formation of discrete polygons via (c) bKL or (d) T-junction cohesion based on similar one-strand motifs, K1 or T1, respectively. The schemes were drawn with the computer software Tiamat.^[33] Red represents the 6-nt base pairing regions and green represents the A3-region and T4-loop for K1 and T1, respectively.

each motif: a blunt end and a hairpin for K1 and T1, respectively. Upon bKL or T-junction cohesion, the motifs will homo-oligomerize into triangle and square tiles because the motifs are not fully rigid. We first tested the assembly by native polyacrylamide gel electrophoresis, nPAGE (Figure 2a). Upon thermal annealing, 1000 nM K1 and T1 each readily homo-oligomerized into primarily two complexes, which appeared as two bands: one fast moving, major band and a slow moving, minor band, presumably corresponding to triangles (homotrimers) and squares (homo-tetramers), respectively. The reasoned geometries of the products were consistent with direct visualization with atomic force microscopy, AFM (Figures 2b and 2c). After annealed, the DNA samples were deposited onto mica surface and immediately imaged in fluid. Under AFM, DNA particles were randomly scattered on the mica surfaces. All particles clearly exhibited the geometries of either triangles or squares. There were many triangles, but few squares, which agreed well with the nPAGE observation (Figure 2a). From the AFM images (Figures S2a–d), we counted both triangles and squares and calculated their relative abundance, which changed as the DNA concentration changed (Figure 2c). As expected, when DNA concentration increased, the relative abundance of the squares (the large complexes) increased. But overall, the squares were the minor products in this DNA concentration range.

Then we investigated the impact of tile-tile interaction on the tile formation. The DNA polygon tiles from motif K1 have multiple blunt ends exposed. Two polygon tiles could interact with each other via one pair of blunt end stacking. In free solution, such blunt-end stacking was too weak to stably

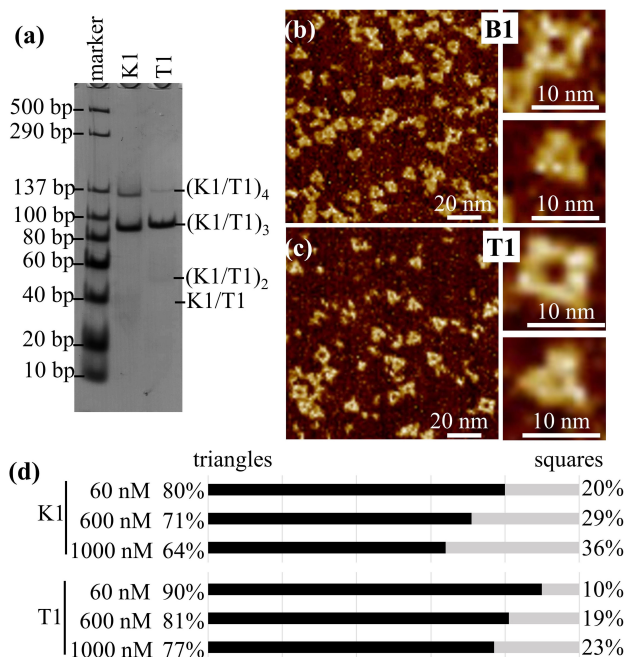


Figure 2. Characterization of the assembly of discrete DNA polygons via homo-oligomerizations in solution. (a) A native polyacrylamide gel electrophoresis (nPAGE) analysis of the DNA assembly ([DNA]: 1000 nM). AFM analysis of the DNA discrete structures homo-polymerized from 60 nM K1 (b) or T1 (c) in solution via bKL and T-junction cohesion, respectively. Each contains a pair of close-up views of individual DNA triangle and square. (d) A bar graph showing the relative distribution of triangle and square at different DNA concentrations. The data for 60 nM and 600 nM were from AFM imaging and the data from 1000 nM was from nPAGE.

associate the DNA tiles together to form any large nanostructure. However, when directly annealing the DNA motifs on mica surface, the situation changes. Our previous study demonstrated that weak DNA tile-tile interaction could be stabilized by DNA-solid surface interaction to allow DNA tiles to assemble into large nanostructures.^[36] We annealed 60 nM K1 on mica surfaces and then imaged the samples by AFM (Figures 3 and S3). As expected, the DNA polygon tiles associated with each other into 2D arrays. Since the motif K1 primarily assembled into triangle tiles, it was expected to see honeycomb-like 2D arrays; instead, to our surprise, tetragonal DNA arrays were observed. This indicated that K1 first assembled into squares instead of triangles. From this, we reasoned that the packing of tiles into 2D arrays impacted the formation of the tiles themselves. In tetragonal lattices, four tiles would form a stable, closed ring; in honeycomb lattices, a stable, closed ring required six tiles. Thus, kinetically, tetragonal lattices are much easier to form than honeycomb lattice in dilute DNA concentrations. Such a preference in lattice formation could mean a shift in the triangle-square equilibrium in tile formation to favor the square formation.

As a control, we annealed 60 nM T1 on mica surface in the same way (Figures 3g and 3h). Polygon tiles from T1 have hairpins instead of blunt ends at outside, thus, could not interact with each other and would remain as individual tiles. Indeed, the observed structures are dominantly individual

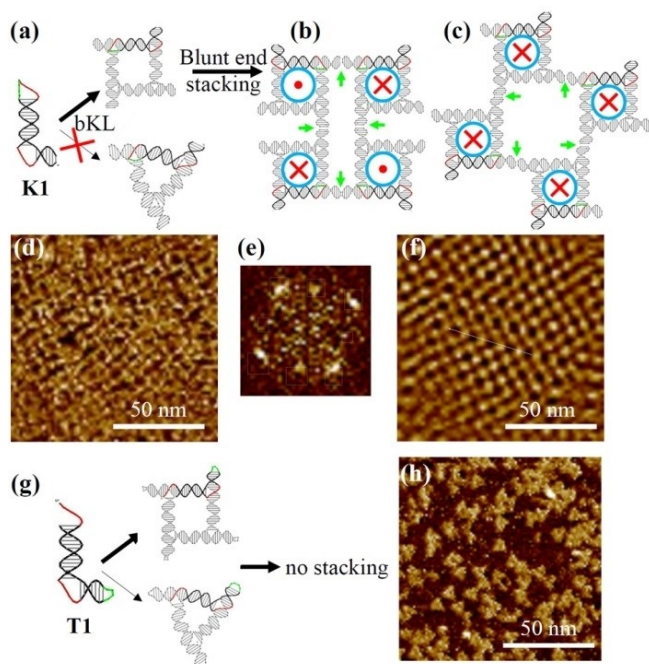


Figure 3. DNA Homo-oligomerization on mica surface. (a) Route of K1 homo-tetramerization into squares, which further interact with each other via blunt end stacking into 2D arrays (b and c). Red crosses and dots indicate that tiles facing into or out of the plane. Green arrows indicate the positions where blunt-end stacking between tiles. (d) An AFM image of the 2D arrays, (e) its corresponding FFT pattern, and (f) the reconstructed image. (g) T1 motif homo-oligomerizes into polygons that have no blunt end, thus remains as individual polygons. (h) An AFM image of the DNA polygons from T1.

triangles and very few squares. This control experiment excluded the possibility that mica surface itself changed the triangle-square equilibrium in tile formation and confirmed our reasoning. To further exclude this possibility, we performed another control experiment where we incubated K1 at a low concentration (60 nM) on the mica surface for an extended time, and we did not find the mica surface rearranging the square motifs and expelling the triangle motifs, but instead a mixture of triangles and squares (Figure S4). This gave more evidence to the possibility that the 2D array was impacting the formation of these component tiles.

Based on the observation above, we optimized the DNA design for assembly of tetragonal DNA arrays from bKL interaction (Figures 4 and S5). When K1 motif is used, the DNA square could potentially interact with other via two competitive ways for blunt-end base-stacking (Figures 3a and 3b). Such a competition prevented the DNA tiles to uniformly interact with each other to form large, highly ordered 2D arrays. To overcome this problem, we replaced the blunt ends with short sticky ends (2- or 4-nt for motif K1a and K1b, respectively) so that any two interacting square tiles had a uniform, relative twisting phase. After annealing the DNA tiles with mica surface, ordered tetragonal 2D arrays were observed and gave out clear fast Fourier transform patterns.

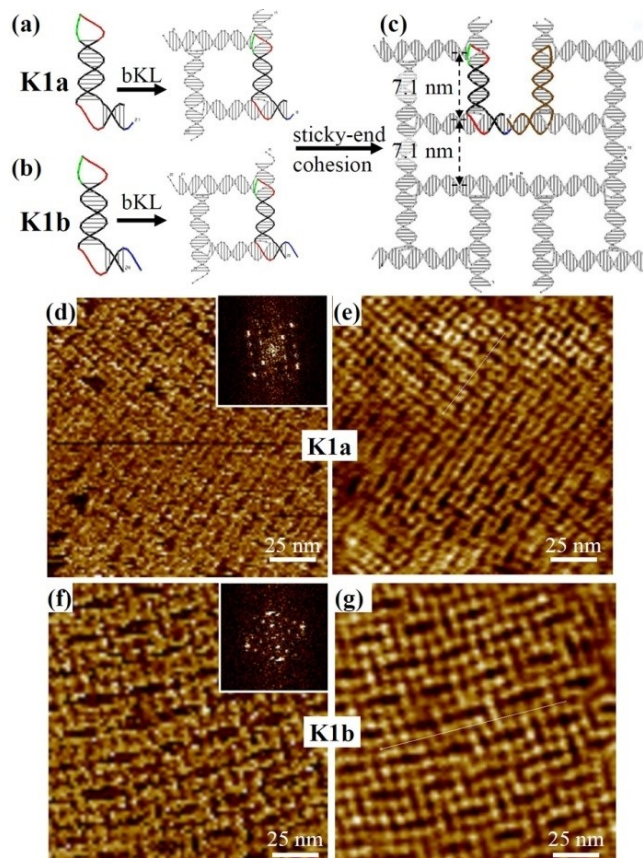


Figure 4. Sticky-end cohesion arranges DNA polygons into 2D arrays on mica surface. Motifs K1a and K1b contain a 2- and 4-nt sticky end, respectively. A pair of an AFM image of tetragonal DNA 2D arrays (inset: FFT pattern) and its reconstructed image from FFT. (d, e) from K1a; (f&g) from K1b.

Conclusion

In conclusion, we demonstrated that DNA tiles associate into higher-order structures which could impact on the tile formation itself. This study shed new insight on the complexity of programming DNA self-assembly. It also adds a new tool for programming DNA self-assembly and allows for fine tuning the assembly pathway for complicated DNA nanostructures. Being able to control the equilibrium of DNA assembly may also provide a new mechanism for switching DNA nanostructures in terms of responsive materials^[37,38] and act as a new platform for biosensing.^[39–43]

Experimental Section

Formation of DNA complexes

Assembly in solution: DNA strands were dissolved in TA/20 mM Mg^{2+} buffer at designated concentration and was slowly cooled down from 95 °C to 22 °C over 8 hours and then 22 °C to 4 °C for 16 hours in a water bath. The TA/20 mM Mg^{2+} buffer contained

40 mM tris base (pH 8.0), 20 mM acetic acid, and 20 mM magnesium acetate.

Assembly on mica surface: the DNA strands were dissolved in TA/10 mM Mg^{2+} buffer at 600 nM. A piece of freshly cleaved mica was emerged in the DNA solution. Then the solution was slowly cooled down from 95 °C to 22 °C over 8 hours and then 22 °C to 4 °C for 16 hours in a water bath. The TA/10 mM Mg^{2+} buffer contained 40 mM tris base (pH 8.0), 20 mM acetic acid, and 10 mM magnesium acetate.

Tabulation of discrete nanostructures from AFM and PAGE (Figure 2d)

For the AFM: Counts of triangles versus squares were based visual analysis with criteria that the shape could only be counted if it had the total correct number of sides and was clearly distinguishable.

For the gel: Percentage of triangles versus squares were based on the band intensity through ImageJ analysis. The bands for K1 and T1 in the 5% PAGE gel were selected and the band intensities that corresponded to the triangle and square were recorded.

Polyacrylamide gel electrophoresis

Denaturing (20%) PAGE: The gels contained 20% 19:1 acrylamide/bisacrylamide, 8 M urea, and TBE buffer (89 mM tris base, adjusted pH to 8.0, 89 mM boric acid and 2 mM EDTA). The gel was run at 55 °C under 650 V on Hoefer SE 600 electrophoresis system and then was stained with ethidium bromide (Sigma). The major band was cut under UV light and was eluted out. As well, denatured samples prepared in the native PAGE gels were not annealed as per above, but instead, the DNA was added to 8 M urea, heated to 95 °C and then snap-cooled before being inserted into the gel wells.

Native (5%) PAGE: The gels contained 19:1 acrylamide/bisacrylamide, TAE/20 mM Mg^{2+} buffer [40 mM tris base, pH was adjusted to 8.0, 20 mM acetic acid, 2 mM ethylenediaminetetraacetic acid (EDTA) and 24 mM magnesium acetate]. The gels were run at 4 °C at 250 V. Then stained with Stains-All (Sigma) and scanned by an HP scanner (Scanjet 4070 Photosmart). The DNA bands were quantitated using ImageJ software for the 1000 nM DNA samples in Figure 2.

AFM imaging in solution

For samples assembled in solution: DNA sample solution (5 μ L) at the designated concentration (600 nM and 60 nM) was deposited onto a freshly cleaved mica surface, incubated for 1 min, and then 25 μ L of imaging buffer (TA/20 mM Mg^{2+} /5 mM Ni^{2+} , containing 40 mM tris base (pH 8.0), 20 mM acetic acid, 20 mM magnesium acetate, and 5 mM of nickel (II) chloride) was added onto the mica. Imaging was performed on a Bruker Multimode 8 AFM at SCANASYST-FLUID mode with ScanAsyst-Fluid + silicon with nitride layer probe (Bruker). Samples annealed at 600 nM had to be diluted to 60 nM in buffer (TA/20 mM Mg^{2+} , containing 40 mM tris base (pH 8.0), 20 mM acetic acid, and 20 mM magnesium acetate) before 5 μ L of sample was deposited to be able to view individual motifs.

To compare the outcome of the K1 motif and its formation, we also performed a control experiment (Figure S4) which required 30 μ L of sample (K1) annealed in TA/10 mM Mg^{2+} buffer to be incubated on the surface for 36 hours.

For samples assembled on mica surface: After annealing, the mica disc was removed from the solution and one side was dried and

then adhered to the iron substrate. Imaging buffer (30 μ L; TA/10 mM Mg^{2+}) was added to the mica disc and then imaging was performed as the samples assembled from solution.

All experiments were carried out at 22 °C. Fourier transformation was determined by the spectrum 2D analysis tool and the repeating distance was determined by the section analysis tool, both in the program NanoScope Analysis version 1.50.

Supporting Information

Additional experimental data can be found in the Supporting Information.

Acknowledgements

This work was supported by NSF (2025187 and 2107393).

Conflict of Interest

The authors declare no conflict of interest.

Data Availability Statement

Data sharing is not applicable to this article as no new data were created or analyzed in this study.

Keywords: branched kissing loop · DNA nanostructures · DNA motif · T-junction · Two-dimensional arrays

- [1] N. C. Seeman, *Nano Lett.* **2020**, *20*, 1477–1478.
- [2] F. A. Aldaye, A. L. Palmer, H. F. Sleiman, *Science* **2008**, *321*, 1795–1799.
- [3] M. R. Jones, N. C. Seeman, C. A. Mirkin, *Science* **2015**, *347*, 1260901.
- [4] H. Raezani, H. Dietz, *Nat. Rev. Genet.* **2020**, *21*, 5–26.
- [5] J. Dong, C. Zhou, Q. Wang, *Top. Curr. Chem.* **2020**, *33*, 1–25.
- [6] Z. Ge, H. Fu, Q. Li, C. Fan, *J. Am. Chem. Soc.* **2018**, *140*, 17808–17819.
- [7] F. Zhang, J. Nangreave, Y. Liu, H. Yan, *J. Am. Chem. Soc.* **2014**, *136*, 11198–11211.
- [8] N. C. Seeman, *J. Theor. Biol.* **1982**, *99*, 237–247.
- [9] E. Winfree, F. Liu, L. A. Wenzler, N. C. Seeman, *Nature* **1998**, *394*, 539–544.
- [10] H. Yan, S. H. Park, G. Finkelstein, J. H. Reif, T. H. Labean, *Science* **2003**, *301*, 1882–1884.
- [11] P. Wang, S. Gaitanaros, S. Lee, M. Bathe, W. M. Shih, Y. Ke, *J. Am. Chem. Soc.* **2016**, *138*, 7733–7740.
- [12] A. Tandon, Y. Song, S. B. Mitta, S. Yoo, S. Park, S. Lee, M. T. Raza, T. H. Ha, S. H. Park, *ACS Nano* **2020**, *4*, 5260–5267.
- [13] M. Wang, H. Huang, Z. Zhang, S.-J. Xiao, *Nanoscale* **2016**, *8*, 18870–18875.
- [14] W. Wang, T. Lin, S. Zhang, T. Bai, Y. Mi, B. Wei, *Nucleic Acids Res.* **2016**, *16*, 7989–7996.
- [15] Y. Yang, Z. Wu, L. Wang, K. Zhou, K. Xia, Q. Xiong, L. Liu, Z. Zhang, E. R. Chapman, Y. Xiong, T. J. Melia, E. Karatekin, H. Gu, C. Lin, *Nat. Chem.* **2020**, *13*, 335–342.
- [16] P. W. Rothmund, N. Papadakis, E. Winfree, *PLoS Biol.* **2004**, *2*, e424.
- [17] Z. Zhang, J. Song, F. Besenbacher, M. Dong, K. V. Gothelf, *Angew. Chem.* **2013**, *35*, 9389–9393.
- [18] J. C. Mitchell, J. R. Harris, J. Malo, J. Bath, A. J. Turberfield, *J. Am. Chem. Soc.* **2004**, *126*, 16342–16343.
- [19] X. Wang, H. Jun, M. Bathe, *J. Am. Chem. Soc.* **2022**, *144*, 4403–4409.

- [20] D. Minev, C. M. Wintersinger, A. Ershova, W. M. Shih, *Nat. Commun.* **2021**, *12*, 1741.
- [21] J. Li, C. Fan, H. Pei, J. Shi, Q. Huang, *Adv. Mater.* **2013**, *32*, 4386–4396.
- [22] L. Liu, Z. Li, Y. Li, C. Mao, *J. Am. Chem. Soc.* **2019**, *141*, 4248–4251.
- [23] C. Zhang, M. Zheng, Y. P. Ohayon, S. Vecchioni, R. Sha, N. C. Seeman, N. Jonoska, C. Mao, *J. Am. Chem. Soc.* **2022**, *144*, 8741–8745.
- [24] J. Nowakowski, P. J. Shim, G. S. Prasad, C. D. Stout, G. F. Joyce, *Natl. Struct. Biol.* **1999**, *6*, 151–156.
- [25] B. F. Eichman, J. M. Vargason, B. H. M. Mooers, P. S. Ho, *Proc. Natl. Acad. Sci. USA* **2000**, *97*, 3971–3976.
- [26] D. S. Goodsell, A. J. Olson, *Annu. Rev. Biophys. Biomol. Struct.* **2000**, *29*, 105–153.
- [27] J. S. Parker, *Microbiol. Rev.* **1989**, *53*, 273–298.
- [28] F. H. C. Crick, J. D. Watson, *Nature* **1956**, *177*, 473–475.
- [29] H. Zuo, C. Mao, *Adv. Drug Delivery Rev.* **2019**, *147*, 22–28.
- [30] X. Zhang, H. Yan, Z. Shen, N. C. Seeman, *J. Am. Chem. Soc.* **2002**, *124*, 12940–12941.
- [31] M. Zheng, Z. Li, L. Liu, M. Li, V. E. Paluzzi, J. H. Choi, C. Mao, *J. Am. Chem. Soc.* **2021**, *143*, 20363–20367.
- [32] D. Liu, C. W. Geary, G. Chen, Y. Shao, M. Li, C. Mao, E. S. Andersen, J. A. Piccirilli, P. W. K. Rothmund, Y. Weizmann, *Nat. Chem.* **2020**, *12*, 249–259.
- [33] S. Williams, K. Lund, C. Lin, P. Wonka, S. Lindsay, H. Yan, in *International Workshop on DNA-Based Computers*, **2008**, 90–101.
- [34] S. Hamada, S. Murata, *Angew. Chem. Int. Ed.* **2009**, *48*, 6820–6823; *Angew. Chem.* **2009**, *121*, 6952–6955.
- [35] D. Han, X. Qi, C. Myhrvold, B. Wang, M. Dai, S. Jiang, M. Bates, Y. Liu, B. An, F. Zhang, H. Yan, P. Yin, *Science* **2017**, *358*, eaao2648.
- [36] L. Liu, Y. Li, Y. Wang, J. Zheng, C. Mao, *ChemBioChem* **2017**, *18*, 2404–2407.
- [37] Y. Yang, C. Lin, *Science* **2017**, *357*, 352–353.
- [38] M. Zheng, Z. Li, C. Zhang, N. C. Seeman, C. Mao, *Adv. Mater.* **2022**, *34*, 2200441.
- [39] L.-L. Li, P. Wu, K. Hwang, Y. Lu, *J. Am. Chem. Soc.* **2013**, *135*, 2411–2414.
- [40] H. Pei, N. Lu, Y. Wen, S. Song, Y. Liu, H. Yan, C. Fan, *Adv. Mater.* **2010**, *42*, 4754–4758.
- [41] P. S. Kwon, S. Ren, S.-J. Kwon, M. E. Kizer, L. Kuo, M. Xie, D. Zhu, F. Zhou, F. Zhang, D. Kim, K. Fraser, L. D. Kramer, N. C. Seeman, J. S. Dordick, R. J. Linhardt, J. Chao, X. Wang, *Nat. Chem.* **2020**, *12*, 26–35.
- [42] M. Liu, F. Wang, X. Zhang, X. Mao, L. Wang, Y. Tian, C. Fan, Q. Li, *Nat. Protoc.* **2021**, *16*, 383–404.
- [43] M. Bai, F. Chen, X. Cao, Y. Zhao, J. Xue, X. Yu, C. Fan, Y. Zhao, *Angew. Chem. Int. Ed.* **2020**, *32*, 13267–13272.

Manuscript received: May 31, 2022
Revised manuscript received: July 7, 2022
Accepted manuscript online: July 8, 2022
Version of record online: July 27, 2022
